In situ structure of trypanosomal ATP synthase dimer reveals a unique arrangement of catalytic subunits

Classification: Biophysics and Computational Biology

In-situ structure of trypanosomal ATP synthase dimer reveals unique arrangement of catalytic subunits

Alexander W. Mühleip[1], Caroline E. Dewar[2], Achim Schnaufer[2], Werner Kühlbrandt[1]* & Karen M. Davies[1,3]*

[1]Department of Structural Biology, Max Planck Institute of Biophysics, Max-von-Laue Str. 3, 60438 Frankfurt am Main, Germany.

[2]Institute of Immunology & Infection Research and Centre for Immunity, Infection & Evolution, University of Edinburgh, Edinburgh EH9 3FL, UK

[3]present address: Molecular Biophysics and Integrative Bio-Imaging Division, Lawrence Berkeley National Laboratory, Berkeley, CA 94720

*corresponding authors
Werner.Kuehlbrandt@biophys.mpg.de
KMDavies@lbl.gov

Keywords: mitochondrial ATP synthase, electron cryo-tomography, subtomogram averaging, trypanosome, rotary catalysis

Abstract

We used electron cryo-tomography and subtomogram averaging to determine the *in situ* structures of mitochondrial ATP synthase dimers from two organisms belonging to the phylum euglenozoa: *Trypanosoma brucei*, a lethal human parasite, and *Euglena gracilis,* a photosynthetic protist. At 32.5 Å and 27.5 Å resolution, the two structures clearly exhibit a non-canonical F_1 head, in which the catalytic $(\alpha\beta)_3$ assembly forms a triangular pyramid, rather than the pseudo-sixfold ring arrangement typical of all other ATP synthases investigated so far. Fitting of known X-ray structures reveals that this unusual geometry results from a phylum-specific cleavage of the α-subunit, in which the C-terminal α_C fragments are displaced by ~20 Å and rotated by ~30° from their expected positions. In this location, the α_C fragment is unable to form the conserved catalytic interface that was thought to be essential for ATP synthesis, nor can it convert γ-subunit rotation into the conformational changes implicit in rotary catalysis. The new arrangement of catalytic subunits suggests that the mechanism of ATP generation by rotary ATPases is less strictly conserved than has been generally assumed. The ATP synthases of these organisms present a unique model system to dissect the individual contributions of the α- and β-subunits to the fundamental process of ATP synthesis.

Significance

The mitochondrial F_1F_o ATP synthase is an essential membrane protein machine that supplies all eukaryotic cells with ATP. The proton-driven rotation of the rotor assembly in the membrane transmits energy to the catalytic F_1 head, where ATP is generated by rotary catalysis. We determined the *in situ* structures of ATP synthase dimers from the lethal human parasite *Trypanosoma brucei* and its free-living relative *Euglena gracilis.* In both ATP synthases, the catalytic subunits form a threefold pyramid rather than the usual near-sixfold ring. This unexpected finding indicates that the structure of the F_1 head, and therefore its catalytic action, is less highly conserved than previously thought. It provides new insights into the fundamental mechanism of ATP production in higher organisms.

\body **Introduction**

F_1F_o ATP synthases are ancient, energy-converting nanomachines that generate ATP by rotary catalysis (1). In mitochondria, the ATP synthases form rows of dimers along the highly curved ridges of the inner membrane cristae (2, 3). All known F_1F_o (F-type) ATP synthases consist of a catalytic, hydrophilic $(\alpha\beta)_3$ hexamer, a hydrophobic membrane-embedded region containing a rotor ring that is driven like a turbine by the proton gradient, and a pair of stalks that connect the two. The central stalk transmits the torque of the rotor ring to the $(\alpha\beta)_3$ hexamer to power catalysis, while the peripheral stalk acts as a stator to prevent idle rotation of the catalytic subunits with the rotor assembly. The $(\alpha\beta)_3$ subunits and the central stalk make up the membrane-extrinsic F_1 subcomplex. The membrane-intrinsic subunits including the rotor ring and the peripheral stalk form the F_o subcomplex.

The F_1 subcomplex has three catalytic sites, each located at an interface of the α- and β-subunits. The two subunits alternate in the $(\alpha\beta)_3$ hexamer, which forms a ring of near-sixfold symmetry (4). ATP synthesis is powered by the proton-driven rotation of the central stalk, which induces conformational changes in the α- and β-subunits (5, 6). In the course of these changes, a conserved α-subunit arginine inserts into the nucleotide binding pocket of the β-subunit (7). Substitution of the arginine residue inhibits ATP production, highlighting the essential role of the α-subunit in catalysis (8, 9).

Trypanosomes belong to a group of parasitic protists, which cause severe and widespread insect-borne human and animal diseases. Biochemistry and mass spectrometry have indicated that the α-subunit in the mitochondrial ATP synthase of euglenozoa (which include trypanosomes) exists as two separate fragments: an N-terminal 14-kDa fragment (α_N) and a C-terminal 44-kDa fragment (α_c) (10-14). Even though the α-subunit is cleaved, the complex still hydrolyses and synthesizes ATP, which is critical for the survival of *Trypanosoma brucei,* the sleeping sickness parasite (10, 11, 14-19). How the cleavage affects the structure and molecular mechanism of the enzyme is unknown. Here we report the *in situ* structure of the mitochondrial ATP synthase from the 'procyclic' insect stage of the lethal human parasite *T. brucei* and the related *Euglena gracilis,* a photosynthetic protist. The structures were determined by electron cryo-tomography and subtomogram averaging to a resolution of 32.5 Å and 27.5 Å, respectively. Both structures reveal an

unexpected arrangement of the catalytic subunits, which form a triangular pyramid, rather than a hexameric ring of near-sixfold symmetry, as in all other known rotary ATPases. Rigid body fitting of X-ray structures showed that the unusual arrangement of catalytic subunits in the F_1 head results from the phylum-specific cleavage of the α-subunit. The subtomogram averages from both organisms indicate that the α_c fragment is displaced from the central stalk by ~2 nm and forms a link between neighbouring β-subunits. Consequently, the typical catalytic interfaces of rotary ATPases cannot form, and therefore the mechanism of ATP synthesis has to be different.

Results

Structure of euglenozoan ATP synthase dimers *in situ*

Mitochondrial membranes were isolated from procyclic (insect stage) *T. brucei* or light-grown *E. gracilis* cells and imaged by electron cryo-tomography. Tomographic volumes revealed that cristae were discs decorated with double rows of 10-nm particles. The structure of the particles obtained by subtomogram averaging confirmed that they were ATP synthase dimers. A total of 1,294 dimers from *E. gracilis* and 925 from *T. brucei* were averaged to generate maps at 27.5 Å or 32.5 Å resolution (Figure 1; Figure S1, Movie S1). The ATP synthase dimers of both species are twofold-symmetric, V-shaped structures with distances of 24.5 nm between the catalytic F_1 heads in *T. brucei* and 22 nm in *E. gracilis* (Figure 1A, D) and an angle between the long axes of the monomers of 65° in *T. brucei* and 50° in *E. gracilis.* The peripheral stalks are positioned on opposite sides of the dimer and are structurally unrelated to other peripheral stalk subcomplexes (Figure 1B,E)(3, 20). On the lumenal side of the membrane, the monomers are connected by several interlinked protein densities (Figure 1C,F). In the complex from *E. gracilis*, two protein domains near the dimer axis tie the monomers together on the matrix side.

Cleavage of the α-subunit results in an unusual arrangement of catalytic subunits

The most conspicuous feature of the two new ATP synthase dimer maps is the catalytic F_1 head (Figure 2, Figure S2). In all known rotary ATPases, the F_1 head is a hexagonal prism of near-sixfold symmetry, consisting of alternating α- and β-subunits or their equivalents (4, 21-24). In the *T. brucei* and *E. gracilis* ATP synthases, the F_1 head resembles a triangular pyramid (Figure 2A,D; Figure S2A,E). Comparison to the bovine F_1 reveals that the subtomogram average map accommodates only every second subunit of the $(\alpha\beta)_3$ hexamer (Figure 2B,E; Figure S2B,C; Figure S3). The densities of the three other intervening subunits are arc-shaped and look strikingly different from those in the bovine or yeast F_1 heads.

Previous mass spectrometry and biochemical studies indicated that the α-subunit of euglenozoan ATP synthases exists as two separate fragments (α_N and α_C) (10-13). To investigate whether the cleavage of the α-subunit might account for the unusual structure of the F_1 head, we fitted a cleaved model of the bovine F_1 structure into the subtomogram average densities (Figure 2B,E, Figure S2C,G). The α-subunit is cleaved by an unidentified

protease in a sequence found only in euglenozoa (residues 145-169 in *T. brucei*) (10, 13). This cleavage site maps to a loop that connects the N-terminal β-barrel to the central domain of the bovine α-subunit (Figure 2G, H). We severed the α-subunit of the bovine $(\alpha\beta)_3$ atomic model (4) at this location and positioned the resulting subcomplex (β + α_N subunits) into the EM maps as a rigid body. In both subtomogram averages, the atomic model matched the density well, with the N-terminal β-barrels from both the α_N fragment and the β-subunit occupying a narrow ring of density below the OSCP, known as the crown region. The remainder of the β-subunits occupied the three densities adjacent to the central stalk (Figure 2B,E; Figure S2C,G).

The fit of the α_N and β-subunits did not occupy the volumes of the arc-shaped densities, which form the vertices of the triangular pyramid (blue densities, Figure2B,E; Figure S2C,G). These densities span the gap between neighbouring β-subunits and are 10 nm long and approximately 2 nm wide and enclose a volume of approximately $49 \cdot 10^3$ Å^3 and $58 \cdot 10^3$ Å^3 in *E. gracilis* and *T. brucei*. Based on an average partial specific volume of 1.2 Å^3/Da (25), each arc-shaped density should accommodate a protein with a molecular mass of 41-48 kDa. This is very similar to the size of the α_C fragment (44 kDa), which in *T. brucei* has been shown to remain bound to the F_1 subcomplex, as demonstrated by α_C-specific antisera (26) and mass spectrometry (10). To assess whether the cleaved α_C fragments could be located in the arc-shaped densities, we performed rigid body fitting (Figure 2C,F; Figure S2D,H; Movie S2). The α_C fragments fitted the profiles of the arc-shaped density well, indicating that they do indeed constitute the vertices of the triangular F_1. Despite the good overall match, rigid body fitting permits several possible orientations of the α_C fragment (Figure S4). We consider the α_C fragment position that involves an outward displacement of ~20Å and a rotation by 30° as most likely (Figure 2C,F; Figure S2D,H), because it requires the minimal offset from the canonical structure. The accuracy of the fit is limited by the map resolution. Nevertheless, based on our difference map (Figure S3B,D), the rigid-body fits (Figure 2C,F; Figure S2D,H) and the fact that the α_C fragment remains attached to the F_1 subcomplex after cleavage (10, 26), we can unambiguously assign the α_C fragments to the arc-shaped densities. Thus, our results show that in euglenozoa, cleavage of the mitochondrial α-subunit results in an unusual arrangement of catalytic subunits in a triangular F_1

pyramid. We conclude that the structure of the catalytic F_1 head in euglenozoa is substantially different from that of any other known rotary ATPase.

To assess whether the *in situ* structures obtained by subtomogram averaging are of an active complex, we solubilised samples of the *E. gracilis* mitochondrial membranes used for cryo-ET with n-dodecyl β-D-maltoside (DDM) and performed blue native gel electrophoresis (BN-PAGE). Two bands reacted to an in-gel ATPase activity assay, one in the megadalton range, which is the ATP synthase dimer, and the other around ~700 kDa which is the ATP synthase monomer (Figure S5). These results indicate that the ATP synthases averaged in the tomograms of isolated mitochondrial membranes from *E. gracilis* are catalytically active.

Dimer rows in *Euglena* and trypanosomes indicate an unexpected arrangement of ATP synthase monomers

To determine the macromolecular arrangement of ATP synthase dimers from *E. gracilis* and *T. brucei* in the membrane, the subtomogram averages were placed into the original tomographic volumes in the positions and orientations determined in the averaging process. In both species, the isolated mitochondrial membranes were decorated with multiple ATP synthase dimer rows that are arranged in short left-handed helix segments around the edges of discoid vesicles (Figure 3A-H; Movie S3). Each row contained between three to six dimers. The short dimer rows encompass the entire circumference of the disk-shaped membranes (Figure 3D, H).

In each row, the two F_1 monomers from one dimer interdigitate with monomers from the next dimers along the row. As a result, the nearest neighbour monomers, both across and along the row, belong to different dimers (Figure 3I,L). This contrasts with the arrangement of ATP synthase dimers in metazoans and fungi, where the nearest monomers across the row belong to the same dimer (3). When viewed from the lumen, the dimers form a ladder-like assembly (Figure 3C,G, K,N). When each row is examined in isolation, the principal curvature is caused by the association of dimers into rows rather than by the dimers themselves (Figure 3J, M). The resulting membrane curvature is stronger in *T. brucei* than in *E. gracilis* (Figure 3J,M), most likely due to the different dimer angles in the two species (Figure 1A, D).

Discussion

Structural variation of mitochondrial ATP synthase dimers and dimer rows

The assembly of the mitochondrial ATP synthase into dimers, and of dimers into rows, is a feature common to mitochondria of all species examined to date (2, 3, 27-29). The principal role of dimer rows appears to be in the formation of mitochondrial inner membrane cristae. Tomographic analysis has revealed two different row architectures, which bend the membrane in different ways. The first type of row architecture, which we refer to as the metazoan type, is found in metazoans, plants and fungi. In this group, the ATP synthases form V-shaped dimers with a dimer angle of ~90° between monomers (3). Dimers of the metazoan type assemble into straight rows along the edges of lamellar cristae, without any lateral offset between adjacent dimers (3). The V-shape of individual dimers induces a sharp, local 90°-membrane curvature which is responsible for driving the self-association of dimers into rows and shaping of cristae membranes (30, 31).

In ciliates (29), euglenozoa (this study) and green algae (20), the ATP synthase dimers form a left- or right-handed helix along the curved ridges of the cristae or along the outer perimeter of helical tubular cristae. In these organisms, the principal membrane curvature is caused by the macromolecular association of dimers into helical arrays, rather than by the individual dimers, as in metazoans (Figure 3J, M). It will be interesting to investigate the architecture of ATP synthase complexes in the bloodstream stage of *T. brucei,* which lacks oxidative phosphorylation and contains sparse, if any mitochondrial cristae (32) and uses the enzyme as an ATP-powered proton pump to generate the mitochondrial membrane potential (16, 18).

A striking difference between the metazoan-type ATP synthase dimers and that of protozoans or unicellular algae, which we refer to as the protozoan type, is the structural diversity of the peripheral stalk and dimer interfaces (33). The architecture of all metazoan-type ATP synthase dimers studied so far is virtually identical (3), and sequence analysis and proteomics have identified homologous subunits for nearly all the subunits that constitute the mitochondrial ATP synthase in these organism (34, 35). In contrast, there seem to be no subunits in the protozoan-type ATP synthases that correspond to the peripheral stalk or dimer interface in the metazoan type. Instead, proteomics and biochemical analysis have identified several unique subunits, none of which are

homologous between the various phyla (10, 11, 36, 37). This variation in subunit composition correlates with the observed diversity in structure, which may reflect adaptation to different energetic requirements or environmental conditions. Apparently, this adaptation occurred before trypanosomes adopted their parasitic lifestyle.

Unusual arrangement of catalytic subunits in the F_1 head of euglenozoan ATP synthase dimers

Despite the diversity of ATP synthase dimer architectures observed in different species, the catalytic subunits that are involved in ATP synthesis and form the F_1 subcomplex are structurally conserved in all previously reported structures (36, 38, 39). Here, we show that the catalytic F_1 head of the mitochondrial ATP synthase dimers from *E. gracilis* and *T. brucei* exhibits an unprecedented pyramidal structure (Figure 2 and Figure S2). This unusual arrangement of catalytic subunits is surprising, given the otherwise strictly conserved pseudo-sixfold symmetry and catalytic mechanism of the $(\alpha\beta)_3$ hexamer in all other known F-type ATPases, including those of bacteria and chloroplasts (4, 24, 40). The observed alterations in the *T. brucei* and *E. gracilis* F_1 region are in line with previous biochemical studies that reported a complete cleavage of the α-subunit into two fragments, both of which remain bound to the ATP synthase (10-14). Furthermore, it has been shown that despite the α-subunit fragmentation, the *T. brucei* ATP synthase remains catalytically active throughout the life cycle and is essential for parasite survival in both the procyclic and bloodstream form (10, 16, 18, 19); as mentioned above, it is the reverse function as a proton-pumping ATPase that is essential for survival in the mammalian host. Additionally, the isolated mitochondrial membranes from *E. gracilis* isolated in this study contained catalytically active ATPase, as demonstrated by in-gel activity (Figure S5).

In the bovine ATP synthase, the catalytic sites are located at the interface of the α- and β-subunits (Figure 4C). The nucleotide binding sites are largely formed by the central domain of the β-subunits, while the α-subunits contribute a conserved arginine (the arginine finger) that is essential for catalysis (Figure 4C,F)(8). In euglenozoa, the nucleotide binding site in the β-subunit is conserved (13), but the α/β interface is not (Figure 2B, E; Figure S2C,G). However, in the unusual arrangement of catalytic subunits, it appears unlikely that the arginine in the α-subunit, which is present in *T. brucei* and *E. gracilis*, can reach the bound nucleotide from its remote position in the central domain

of the α_c fragment (Figure 4D, E). Because the arginine finger is critical for catalysis in both the ATP synthase (8) and in many other ATPase domains in general (e.g. AAA+ ATPases (41)), it has to be located at the active site and thus must be contributed by a different part of the structure. Apart from a suitably positioned residue in the α_c fragment, a prime candidate is the euglenozoa-specific F_1 subunit p18 (10-13) (systematic ID in *T. brucei* Tb927.5.1710). Knockdown of p18 in procyclic *T. brucei* by RNAi has been shown to result in slowed growth and a disappearance of F_1, indicating that p18 is required for F_1 integrity (42). Although functional data on the role of p18 in other trypanosomatids has not been reported so far, it is a subunit of the mitochondrial ATP synthase in other trypanosomatids, including *Leishmania tarentolae* (13) and *Crithidia fasciculata* (12), as well as in the euglenoid *E. gracilis* (11), strongly suggesting that this subunit is generally conserved in euglenozoa. The location of p18 in the unusual F_1 structure is currently unknown. However, an unassigned density region between α_N and α_C and the likely presence of more than one copy of p18 per F_1 molecule (10) suggest that this region may contain p18 (Figure S6). To resolve the question of how the euglenozoan ATP synthase dimers produce ATP requires a higher-resolution structure.

In *situ* structure of euglenozoan ATP synthase dimers provides novel insights into rotary catalysis

ATP synthesis by rotary catalysis involves three key stages: 1) proton movement across the membrane-embedded F_o sector drives the rotation of the central stalk, 2) rotation of the central stalk causes conformational changes at the catalytic α/β interface, which triggers phosphate bond formation, and 3) conformational changes are cooperatively transmitted between catalytic sites. The exact molecular mechanism of this process is not understood. A central question is the extent to which each of the α- and β-subunits contribute to this process. In the euglenozoan ATP synthase, the contributions of each subunit to rotary catalysis can be dissected. The displacement of the α_C fragments away from the central stalk means that the γ-subunit is unable to interact with the α-subunits directly (Figure 4A,B). Thus, at least in the euglenozoan ATP synthase, but possibly also in the conserved F_1 structure, interactions between the β- and γ-subunit are sufficient for the conversion of γ-subunit rotation into conformational changes in the process of mechanochemical coupling.

The different position of the α_C fragments in the euglenozoan ATP synthase also rules out the involvement of the γ-subunit in the transmission of conformational changes between catalytic sites, as it can only interact with one β-subunit at a time. This observation is consistent with results of high-speed atomic force microscopy, which demonstrated that in *Bacillus* PS3, conformational transmission between catalytic sites does not require the central stalk; however loss of a single α-subunit stops the propagation of conformational changes (43). In the *T. brucei* and *E. gracilis* structures, the central and C-terminal domains of the α-subunit are displaced from their canonical position but remain bound to the complex, indicating an essential role of the fragment in enzymatic activity. In these complexes, the α_C fragment connects the C-terminal domain of one β-subunit to the central domain of the neighbouring subunit (Figure 2C; Figure S2D). In the bovine complex, the distance between these two contact points in one β-subunit changes significantly during nucleotide binding and release (4). Therefore, the arc-shaped α_c fragments in the euglenozoan complexes probably transmit conformational changes from one β-subunit to the next, ensuring cooperativity between the three catalytic sites in the F_1 head.

Conclusion

Electron cryo-tomography of mitochondria from *E. gracilis* and insect stage *T. brucei* shows that the ATP synthases of both organisms form dimers, which assemble into short left-handed helical arcs around the edge of disk-shaped cristae. Subtomogram averaging of the ATP synthase dimers in these species revealed a non-canonical F_1 head structure. This unusual structure is the result of a proteolytic cleavage of the α-subunit, which causes a displacement of the central and C-terminal domains of the α-subunit from their canonical position. The structure of the euglenozoan F_1 heads provides new insights into the mechanism of rotary catalysis, in particular how rotation of the central stalk induces conformational changes and how these changes are transmitted between catalytic sites. The so far unique structure of the F_1 head of the euglenozoan ATP synthases represents a potential model system for establishing future in depth studies into dissecting the mechanism of ATP synthesis - a fundamental and essential life process.

Materials and Methods

Culture conditions and sample preparation

T. brucei procyclic form cells (strain 29.13 (44)) were grown at 27°C and 5% (v/v) CO_2 in SDM-79 medium (45) containing hemin (7.5 mg/ml) and 10% (v/v) foetal bovine serum (Gibco, Carlsbad, USA). Cells were counted with a Z2 Cell Counter (Beckman Coulter, Brea,USA) and harvested by centrifugation at 1,200 rpm, 5 min. 600 x 10^6 cells were resuspended in 1.5 ml homogenization buffer (20 mM Tris pH 7.4, 250 mM sucrose, 5 mM $MgCl_2$) and homogenized by 350 passages in a ball-bearing cell homogenizer with 4 µm clearance (Isobiotec, Heidelberg, Germany). The cell lysate was centrifuged at 500 g for 10 min, 4°C. Mitochondrial membranes were pelleted by centrifugation at 16,000 xg for 10 min at 4°C.

E. gracilis (Lebendkulturen Helbig, Prien am Chiemsee, Germany) cultures were grown in *Euglena* medium (46) under a cycle of 10 h of light at 10,000 lx and 14 h of darkness at 21°C. 100-ml cultures were harvested by centrifugation at 800 xg, 10 min, 4°C and resuspended in 10 ml homogenization buffer (20 mM Tris pH 7.4, 250 mM sucrose, 5 mM $MgCl_2$). Cells were homogenized by 30 passages in a cell homogenizer with 8-µm clearance and the homogenate was centrifuged at 1,500 xg, 5 min, 4°C. The supernatant was collected and centrifuged at 6,000 xg, 10 min, 4°C. The resulting pellet contained an upper green layer, which was carefully removed and discarded, and a brownish pellet containing the mitochondrial membranes.

BN-PAGE of solubilised membranes complexes and in-gel ATPase activity assay

E. gracilis mitochondrial membranes were resuspended in solubilisation buffer (final concentration 50 mM Tris/HCl pH 8.0, 1 mM $MgCl_2$ with complete protease inhibitor cocktail (Roche) added), mixed with DDM in a final detergent-to-protein ratio (DPR) of 1:1 (w/w) or 5:1 (w/w) and incubated for 30 min on ice. Samples were centrifuged at 15,000 xg for 15 min, 4°C and solubilised protein complexes were collected from the supernatant. Solubilised *E. gracilis* mitochondrial membranes protein complexes were separated by BN-PAGE as described by Wittig et al. (47), using 3-12% NativePAGE™ Novex® Bis-Tris gradient gels (Life Technologies), which were subsequently stained with Coomassie blue R-250. In-gel ATPase activity assays were performed as previously

described (48), with slight modifications. After gel electrophoresis, native gels were rinsed twice in ddH_2O and once in 1 M Tris/HCl pH 7.8, before incubation in activity buffer (35 mM Tris/HCl pH 7.8, 14 mM $MgSO_4$). ATP, lead (II) nitrate and N,N-Dimethyl-n-dodecylamine N-oxide (LDAO) were added in trace amounts, whereupon white lead phosphate precipitate formed inside the protein bands with ATPase activity during overnight incubation.

Electron cryo-tomography and tomogram processing

Mitochondrial membrane pellets were resuspended in 50 µl freezing buffer (20 mM Tris pH 7.4, 250 mM trehalose) and mixed 1:1 with 6-nm colloidal gold fiducial markers (Aurion, Wageningen, The Netherlands). 3 µl were applied to a glow-discharged 2/2 Cu 300 mesh holey carbon-coated support grid (Quantifoil, Jena, Germany). Excess liquid was removed by blotting (#4 Whatman paper, Sigma-Aldrich, St. Louis, USA) and the grid was rapidly frozen in liquid ethane using a home-built guillotine. Frozen-hydrated specimens of *T. brucei* mitochondrial membranes were imaged in a Titan Krios electron microscope (FEI, Hillsboro, USA) at a nominal magnification of 42,000x, (specimen pixel size, 3.35 Å). Tomographic tilt series were collected at 4 µm defocus to ±60° in 2° increments, starting at +24°. *E. gracilis* mitochondrial membranes were imaged in an FEI Tecnai Polara at a nominal magnification of 90,000x (specimen pixel size, 2.28 Å) and tilt series were collected at 3 µm defocus from -50° to +60° in 2° increments, starting at +24°. In both cases, tilt series were collected using the program LATITUDE (Digital Micrograph, Gatan, Pleasanton, USA). The cumulative dose of a tilt series was ~100 electrons/$Å^2$. Both microscopes were operated at 300 kV and equipped with a Quantum Energy filter and a K2 summit direct electron detector (Gatan) operated in counting mode. Tomographic volumes were reconstructed using IMOD (49). The CTF was estimated and corrected in IMOD (50). The handedness of tomographic volumes was determined by evaluating the tilt axis rotation angle in tilt series of a sample of known handedness. For three-dimensional visualization, tomographic volumes were contrast-enhanced by nonlinear anisotropic diffusion filtering (51) and segmented manually with AMIRA (FEI). Subtomogram averages were placed into original tomographic volumes using the EMPackage plugin (52) for AMIRA.

Subtomogram averaging

ATP synthase dimers were averaged as described (3). Briefly, particle pairs were manually identified in tomographic volumes and initial rotation angles were assigned based on the F_1 head positions relative to the membrane in SPIDER (53). Particles were extracted, rotated and averaged to create an initial reference. Particle alignment was optimized iteratively in PEET (54), using a restricted search range. Resolution of final maps was estimated by Fourier shell correlation (FSC). Particle sets were randomly split into two halves after alignment. The resulting half maps were multiplied with a Gaussian mask before FSC. To prevent mask bias, tomographic volumes were phase-randomized beyond 40 Å using PEET and two half maps were generated by extracting, aligning and averaging the same particle subsets. The FSC curves of the phase-randomized half sets indicated a drop at the randomization frequency. 3D visualization, rigid body fitting and generation of the difference map were performed in UCSF Chimera (55).

Sequence alignment

Sequence alignment was performed with ClustalW2 (56). Sequences were obtained from TriTrypDB (57), UniProt (58) and Perez et al. 2014 (11).

Acknowledgements

We thank Deryck Mills for maintaining the EM facility, and Özkan Yildiz and Juan Francisco Castillo Hernandez for maintaining the computer system. This work was funded by the Max Planck Society (WK), the DFG-funded Cluster of Excellence Frankfurt "Macromolecular Complexes" (KMD) and the UK Medical Research Council grant G0600129 (AS).

Author Contributions

KMD and AWM designed experiments, AWM & CD performed experiments, AWM, & KMD analysed data, and KMD, AWM, WK & AS wrote the paper.

Data deposition

Subtomogram averages of the mitochondrial ATP synthase dimers from *T. brucei* and *E. gracilis* have been deposited in the Electron Microscopy Data Bank under accession codes EMD*** and EMD***, respectively.

Conflict of Interest

The authors declare that they have no conflict of interest.

References

1. Boyer PD (1993) The binding change mechanism for ATP synthase--some probabilities and possibilities. *Biochim Biophys Acta* 1140(3):215-250.
2. Strauss M, Hofhaus G, Schröder RR, & Kühlbrandt W (2008) Dimer ribbons of ATP synthase shape the inner mitochondrial membrane. *EMBO J* 27(7):1154-1160.
3. Davies KM*, et al.* (2011) Macromolecular organization of ATP synthase and complex I in whole mitochondria. *Proc Natl Acad Sci USA* 108(34):14121-14126.
4. Abrahams JP, Leslie AG, Lutter R, & Walker JE (1994) Structure at 2.8 Å resolution of F_1-ATPase from bovine heart mitochondria. *Nature* 370(6491):621-628.
5. Duncan TM, Bulygin VV, Zhou Y, Hutcheon ML, & Cross RL (1995) Rotation of Subunits during Catalysis by *Escherichia coli* F_1-ATPase. *Proc Natl Acad Sci USA* 92(24):10964-10968.
6. Sabbert D, Engelbrecht S, & Junge W (1996) Intersubunit rotation in active F-ATPase. *Nature* 381(6583):623-625.
7. Menz RI, Walker JE, & Leslie AGW (2001) Structure of bovine mitochondrial F_1-ATPase with nucleotide bound to all three catalytic sites: Implications for the mechanism of rotary catalysis. *Cell* 106(3):331-341.
8. Komoriya Y*, et al.* (2012) Principal role of the arginine finger in rotary catalysis of F_1-ATPase. *J Biol Chem* 287(18):15134-15142.
9. Yukawa A, Iino R, Watanabe R, Hayashi S, & Noji H (2015) Key Chemical Factors of Arginine Finger Catalysis of F_1-ATPase Clarified by an Unnatural Amino Acid Mutation. *Biochemistry* 54(2):472-480.
10. Zikova A, Schnaufer A, Dalley RA, Panigrahi AK, & Stuart KD (2009) The F_0F_1-ATP synthase complex contains novel subunits and is essential for procyclic *Trypanosoma brucei*. *PLoS Pathog* 5(5):e1000436.
11. Perez E*, et al.* (2014) The mitochondrial respiratory chain of the secondary green alga *Euglena gracilis* shares many additional subunits with parasitic Trypanosomatidae. *Mitochondrion* 19 Pt B:338-349.
12. Speijer D*, et al.* (1997) Characterization of the respiratory chain from cultured *Crithidia fasciculata*. *Mol Biochem Parasitol* 85(2):171-186.
13. Nelson RE, Aphasizheva I, Falick AM, Nebohacova M, & Simpson L (2004) The I-complex in *Leishmania tarentolae* is an uniquely-structured F_1-ATPase. *Mol Biochem Parasitol* 135(2):221-224.
14. Dean S, Gould MK, Dewar CE, & Schnaufer AC (2013) Single point mutations in ATP synthase compensate for mitochondrial genome loss in trypanosomes. *Proc Natl Acad Sci U S A* 110(36):14741-14746.
15. Bochud-Allemann N & Schneider A (2002) Mitochondrial substrate level phosphorylation is essential for growth of procyclic *Trypanosoma brucei*. *J Biol Chem* 277(36):32849-32854.
16. Schnaufer A, Clark-Walker GD, Steinberg AG, & Stuart K (2005) The F_1-ATP synthase complex in bloodstream stage trypanosomes has an unusual and essential function. *EMBO J* 24(23):4029-4040.
17. Williams N & Frank PH (1990) The mitochondrial ATP synthase of *Trypanosoma brucei*: isolation and characterization of the intact F_1 moiety. *Mol Biochem Parasitol* 43(1):125-132.
18. Brown SV, Hosking P, Li JL, & Williams N (2006) ATP synthase is responsible for maintaining mitochondrial membrane potential in bloodstream form *Trypanosoma brucei*. *Eukaryot Cell* 5(1):45-53.

19. Subrtova K, Panicucci B, & Zikova A (2015) ATPaseTb2, a unique membrane-bound FoF1-ATPase component, is essential in bloodstream and dyskinetoplastic trypanosomes. *PLoS Pathog* 11(2):e1004660.
20. Dudkina NV, Sunderhaus S, Braun HP, & Boekema EJ (2006) Characterization of dimeric ATP synthase and cristae membrane ultrastructure from *Saccharomyces* and *Polytomella* mitochondria. *FEBS Lett* 580(14):3427-3432.
21. Numoto N, Hasegawa Y, Takeda K, & Miki K (2009) Inter-subunit interaction and quaternary rearrangement defined by the central stalk of prokaryotic V_1-ATPase. *EMBO Rep* 10(11):1228-1234.
22. Lau WCY & Rubinstein JL (2012) Subnanometre-resolution structure of the intact *Thermus thermophilus* H^+-driven ATP synthase. *Nature* 481(7380):214-218.
23. Benlekbir S, Bueler SA, & Rubinstein JL (2012) Structure of the vacuolar-type ATPase from *Saccharomyces cerevisiae* at 11-Å resolution. *Nat Struct Mol Biol* 19(12):1356-1362.
24. Shirakihara Y*, et al.* (1997) The crystal structure of the nucleotide-free α3β3 subcomplex of F_1-ATPase from the thermophilic Bacillus PS3 is a symmetric trimer. *Structure* 5(6):825-836.
25. Harpaz Y, Gerstein M, & Chothia C (1994) Volume changes on protein folding. *Structure* 2(7):641-649.
26. Brown BS, Chi TB, & Williams N (2001) The Trypanosoma brucei mitochondrial ATP synthase is developmentally regulated at the level of transcript stability. *Mol Biochem Parasitol* 115(2):177-187.
27. Dudkina NV, Oostergetel GT, Lewejohann D, Braun HP, & Boekema EJ (2010) Row-like organization of ATP synthase in intact mitochondria determined by cryo-electron tomography. *Biochim Biophys Acta* 1797(2):272-277.
28. Daum B, Walter A, Horst A, Osiewacz HD, & Kühlbrandt W (2013) Age-dependent dissociation of ATP synthase dimers and loss of inner-membrane cristae in mitochondria. *Proc Natl Acad Sci USA* 110(38):15301-15306.
29. Mühleip AW*, et al.* (2016) Helical arrays of U-shaped ATP synthase dimers form tubular cristae in ciliate mitochondria. *Proceedings of the National Academy of Sciences of the United States of America*.
30. Davies KM, Anselmi C, Wittig I, Faraldo-Gomez JD, & Kühlbrandt W (2012) Structure of the yeast F_1F_o-ATP synthase dimer and its role in shaping the mitochondrial cristae. *Proc Natl Acad Sci USA* 109(34):13602-13607.
31. Paumard P*, et al.* (2002) The ATP synthase is involved in generating mitochondrial cristae morphology. *EMBO J* 21(3):221-230.
32. Brown RC, Evans DA, & Vickerman K (1973) Changes in oxidative metabolism and ultrastructure accompanying differentiation of the mitochondrion in Trypanosoma brucei. *Int J Parasitol* 3(5):691-704.
33. Lapaille M*, et al.* (2010) Atypical subunit composition of the chlorophycean mitochondrial F_1F_0-ATP synthase and role of Asa7 protein in stability and oligomycin resistance of the enzyme. *Mol Biol Evol* 27(7):1630-1644.
34. Wittig I & Schägger H (2008) Structural organization of mitochondrial ATP synthase. *Biochim Biophys Acta* 1777(7-8):592-598.
35. Eubel H, Jansch L, & Braun HP (2003) New insights into the respiratory chain of plant mitochondria. Supercomplexes and a unique composition of complex II. *Plant Physiol* 133(1):274-286.
36. Balabaskaran Nina P*, et al.* (2010) Highly divergent mitochondrial ATP synthase complexes in *Tetrahymena thermophila*. *PLoS Biol* 8(7):e1000418.

37. van Lis R, Mendoza-Hernandez G, Groth G, & Atteia A (2007) New insights into the unique structure of the F_0F_1-ATP synthase from the chlamydomonad algae *Polytomella sp.* and *Chlamydomonas reinhardtii*. *Plant Physiol* 144(2):1190-1199.
38. Rubinstein JL, Walker JE, & Henderson R (2003) Structure of the mitochondrial ATP synthase by electron cryomicroscopy. *EMBO J* 22(23):6182-6192.
39. Allegretti M*, et al.* (2015) Horizontal membrane-intrinsic α-helices in the stator *a*-subunit of an F-type ATP synthase. *Nature* 521(7551):237-240.
40. Böttcher B & Gräber P (2000) The structure of the H^+-ATP synthase from chloroplasts and its subcomplexes as revealed by electron microscopy. *Biochim Biophys Acta* 1458(2-3):404-416.
41. Ogura T, Whiteheart SW, & Wilkinson AJ (2004) Conserved arginine residues implicated in ATP hydrolysis, nucleotide-sensing, and inter-subunit interactions in AAA and AAA^+ ATPases. *J Struct Biol* 146(1-2):106-112.
42. Hashimi H*, et al.* (2010) The assembly of F_1F_0-ATP synthase is disrupted upon interference of RNA editing in *Trypanosoma brucei*. *Int J Parasitol* 40(1):45-54.
43. Uchihashi T, Iino R, Ando T, & Noji H (2011) High-speed atomic force microscopy reveals rotary catalysis of rotorless F_1-ATPase. *Science* 333(6043):755-758.
44. Wirtz E, Leal S, Ochatt C, & Cross GAM (1999) A tightly regulated inducible expression system for conditional gene knock-outs and dominant-negative genetics in *Trypanosoma brucei*. *Mol Biochem Parasitol* 99(1):89-101.
45. Brun R & Schönenberger (1979) Cultivation and in vitro cloning or procyclic culture forms of *Trypanosoma brucei* in a semi-defined medium. Short communication. *Acta Tropica* 36(3):289-292.
46. Starr RC (1964) Culture Collection of Algae at Indiana University. *Am J Bot* 51(9):1013-1044.
47. Wittig I, Braun HP, & Schägger H (2006) Blue native PAGE. *Nat Protoc* 1(1):418-428.
48. Zerbetto E, Vergani L, & Dabbeni-Sala F (1997) Quantification of muscle mitochondrial oxidative phosphorylation enzymes via histochemical staining of blue native polyacrylamide gels. *Electrophoresis* 18(11):2059-2064.
49. Kremer JR, Mastronarde DN, & McIntosh JR (1996) Computer visualization of three-dimensional image data using IMOD. *J Struct Biol* 116(1):71-76.
50. Xiong QR, Morphew MK, Schwartz CL, Hoenger AH, & Mastronarde DN (2009) CTF determination and correction for low dose tomographic tilt series. *J Struct Biol* 168(3):378-387.
51. Hegerl R & Frangakis AS (2001) Noise reduction in electron tomographic reconstructions using nonlinear anisotropic diffusion. *J Struct Biol* 135(3):239-250.
52. Pruggnaller S, Mayr M, & Frangakis AS (2008) A visualization and segmentation toolbox for electron microscopy. *J Struct Biol* 164(1):161-165.
53. Frank J*, et al.* (1996) SPIDER and WEB: Processing and visualization of images in 3D electron microscopy and related fields. *J Struct Biol* 116(1):190-199.
54. Nicastro D*, et al.* (2006) The molecular architecture of axonemes revealed by cryoelectron tomography. *Science* 313(5789):944-948.
55. Pettersen EF*, et al.* (2004) UCSF Chimera--a visualization system for exploratory research and analysis. *J Comput Chem* 25(13):1605-1612.
56. Larkin MA*, et al.* (2007) Clustal W and clustal X version 2.0. *Bioinformatics* 23(21):2947-2948.
57. Aslett M*, et al.* (2010) TriTrypDB: a functional genomic resource for the Trypanosomatidae. *Nucleic Acids Res* 38:D457-D462.

58. Bateman A, *et al.* (2015) UniProt: a hub for protein information. *Nucleic Acids Res* 43(D1):D204-D212.
59. Böttcher B, Wynne SA, & Crowther RA (1997) Determination of the fold of the core protein of hepatitis B virus by electron cryomicroscopy. *Nature* 386(6620):88-91.
60. Dautant A, Velours J, & Giraud MF (2010) Crystal structure of the Mg·ADP-inhibited state of the yeast F_1c_{10}-ATP synthase. *J Biol Chem* 285(38):29502-29510.

Figure legends

Figure 1: *In situ* structure of mitochondrial ATP synthase dimers in *Euglena gracilis* and *Trypanosoma brucei*

Subtomogram average of ATP synthase dimers from *E. gracilis* (upper row) and *T. brucei* (lower row). Left (A,D), side view; middle, matrix view; right, lumenal view. Dark and light blue, catalytic region; orange, peripheral stalk; red, lumenal density; grey, central stalk; green, oligomycin sensitivity-conferring protein (OSCP). See also Movie S1 and Figure S1. Scale bar 10 nm.

Figure 2: Fit of atomic model to the catalytic region of mitochondrial ATP synthase dimers from *E. gracilis*

(A, B, C) Side views and (D, E, F) matrix views of the F_1 head region in the subtomogram average of *E. gracilis* ATP synthase dimer. (A, D) subtomogram average; (B, E) same with fitted atomic model of the bovine $(\alpha\beta)_3$ hexamer (PDB ID code: 1BMF (4)) without α_c. (C, F) as B and E but with α_c fragments fitted as a rigid body. Dashed line, cross-section plane for Figure 4A,C. (G) Sequence alignment of mitochondrial (mito) α-subunit of *T. brucei, Leishmania major, Crithidia fasciculata, E. gracilis, Bos taurus and Saccharomyces cerevisiae*, and the chloroplast (chloro) α-subunit of *E. gracilis*. Blue, C-terminal sequence of α_N; yellow, N-terminal sequence of α_c; red, non-conserved loop region and region of protease cleavage site in mitochondrial α-subunit of euglenozoa. (H) α-subunit of bovine heart ATP synthase coloured as in (G). Light blue α_N; yellow α_c; red, loop with protease cleavage site; dark blue β-subunit. Scale bar (A-F), 2.5 nm. See also Movie S2, Figure S2 and Figure S3.

Figure 3: Macromolecular arrangement of mitochondrial ATP synthase dimers from *E. gracilis* and *T. brucei in situ*

Tomographic slice through discoid mitochondrial membrane vesicles from *E. gracilis* (A) and *T. brucei* (E) containing ATP synthases (arrowheads). (B, E) Surface representations of (A) and (E) highlighting discoid membranes (blue) and ATP synthase dimer ribbons (yellow and orange). (C, G) Section through the vesicles in (B, F) shows arrangement of ATP synthase dimers viewed from cristae lumen. (D, H) Same as (B, F) but rotated 90°. Scale bar 50 nm. See also Movie S3. (I-N) Row arrangement of ATP synthase dimers as determined from subtomogram averages. (I,L) Matrix view, (J,M) side view, (K, N) lumenal view. (I-K) *E. gracilis,* (L-N) *T. brucei.* Alternating dimers are coloured orange and yellow, and form rows with left-handed helicity (helix axes shown in red). Adjacent ATP synthase monomers in the row belong to different dimers, thus the dimers are interdigitated. Scale bar, 10 nm. See also Movie S3.

Figure 4: Domain arrangement in the catalytic F_1 region

(A,B) Cross section of catalytic domain of *E. gracilis* and *T. brucei* with fitted atomic models as indicated in Fig. 2C; contoured in steps of 0.8 σ. (C) Cross section of the conserved bovine structure (PDB code: 1BMF(4)) for comparison. Blue, β-subunits; yellow α_C fragment; grey, central stalk. Green asterisks, nucleotide binding site in the β-subunits. (D,E,F) Enlarged view of catalytic interface from in *E. gracilis, T. brucei* and *B. taurus* respectively, with arginine finger circled in red and nucleotide binding site in green. Scale bar, 5 nm.

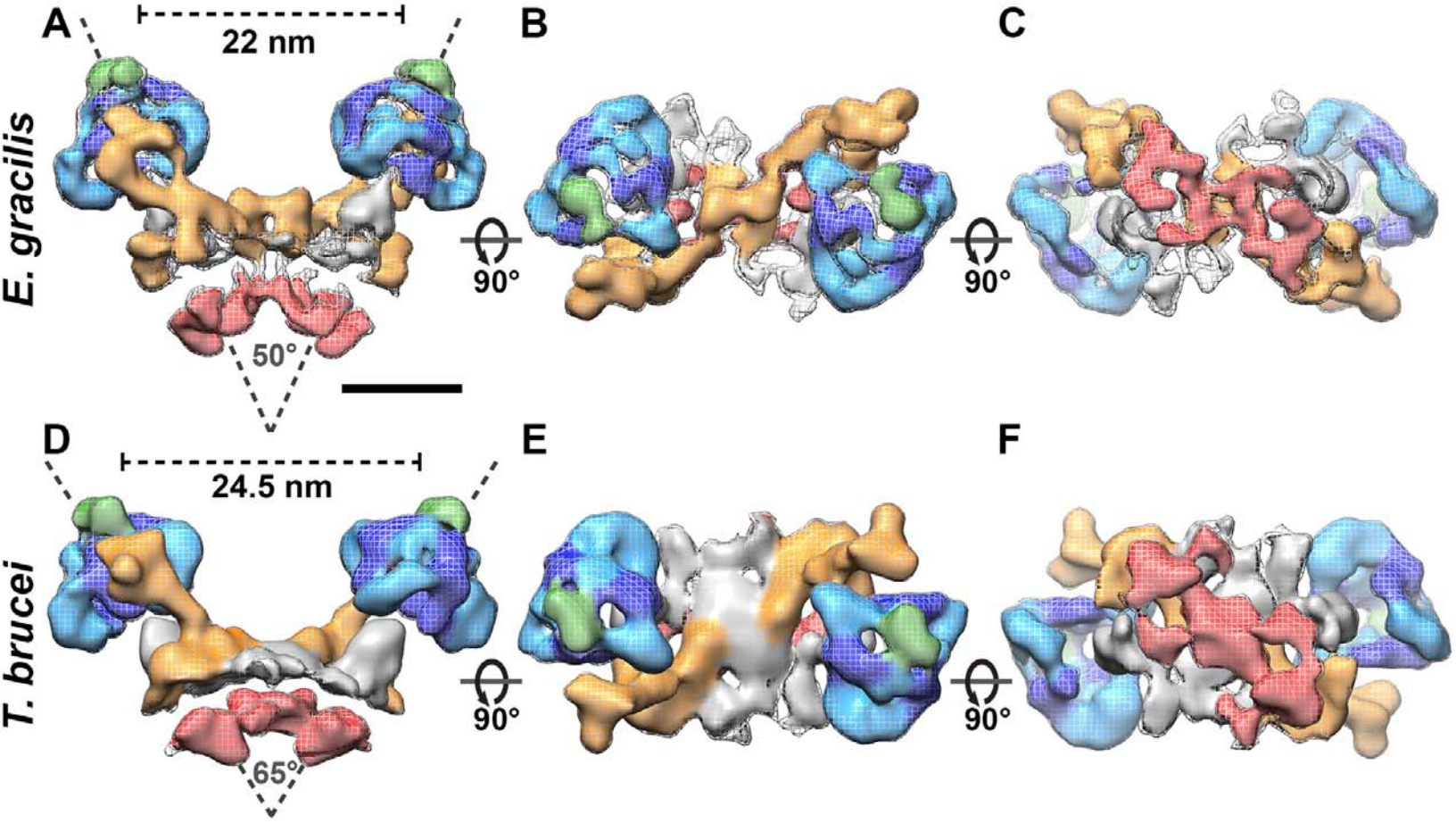
A
22 nm
B
C
E. gracilis
90°
90°
50°
D
24.5 nm
E
F
T. brucei
90°
90°
65°

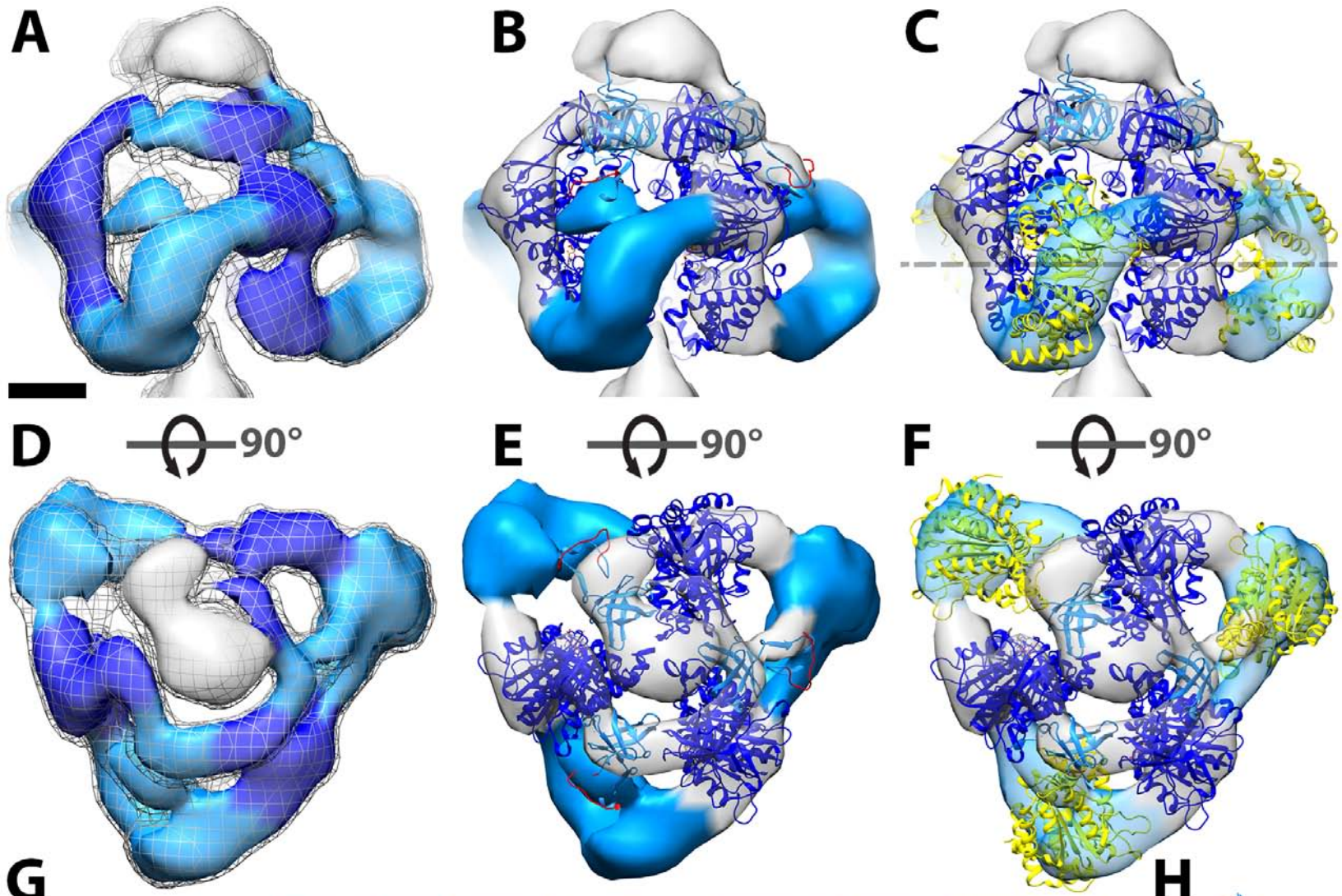

G

```
mito. T. brucei       LGKVVNPLGHEVP-VGLVTRSRRLLDS--TLGKVDTGAPNIV 174
mito. L. major        LGKVVNPLGHEVP-VGLLTRSRALLESEQTLGKVDAGAPNIV 164
mito. C. fasciculata  LGKVVNPLGHEVP-VGLFTRSRALLDSEQVVGKVDAGAPNIV 169
mito. E. gracilis     LGKIINPLGKEIP-TGLFTKAAPLLDDT-KLGLVEEMAPNIV 193
chloro. E. gracilis   LGRVVDALARPIDGKGDIASFT--------TRLIESPAPGIV 138
mito. B. taurus       LGRVVDALGNAIDGKGPIGSKA--------RRRVGLKAPGII 180
mito. S. cerevisiae   LGRVVDALGNPIDGKGPIDAAG--------RSRAQVKAPGIL 174
                      **:::::.*.. :   * .           **.*:
```

H

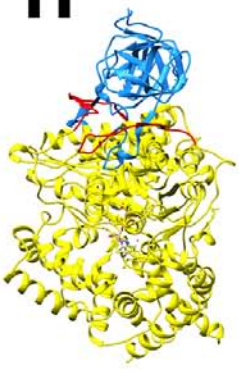

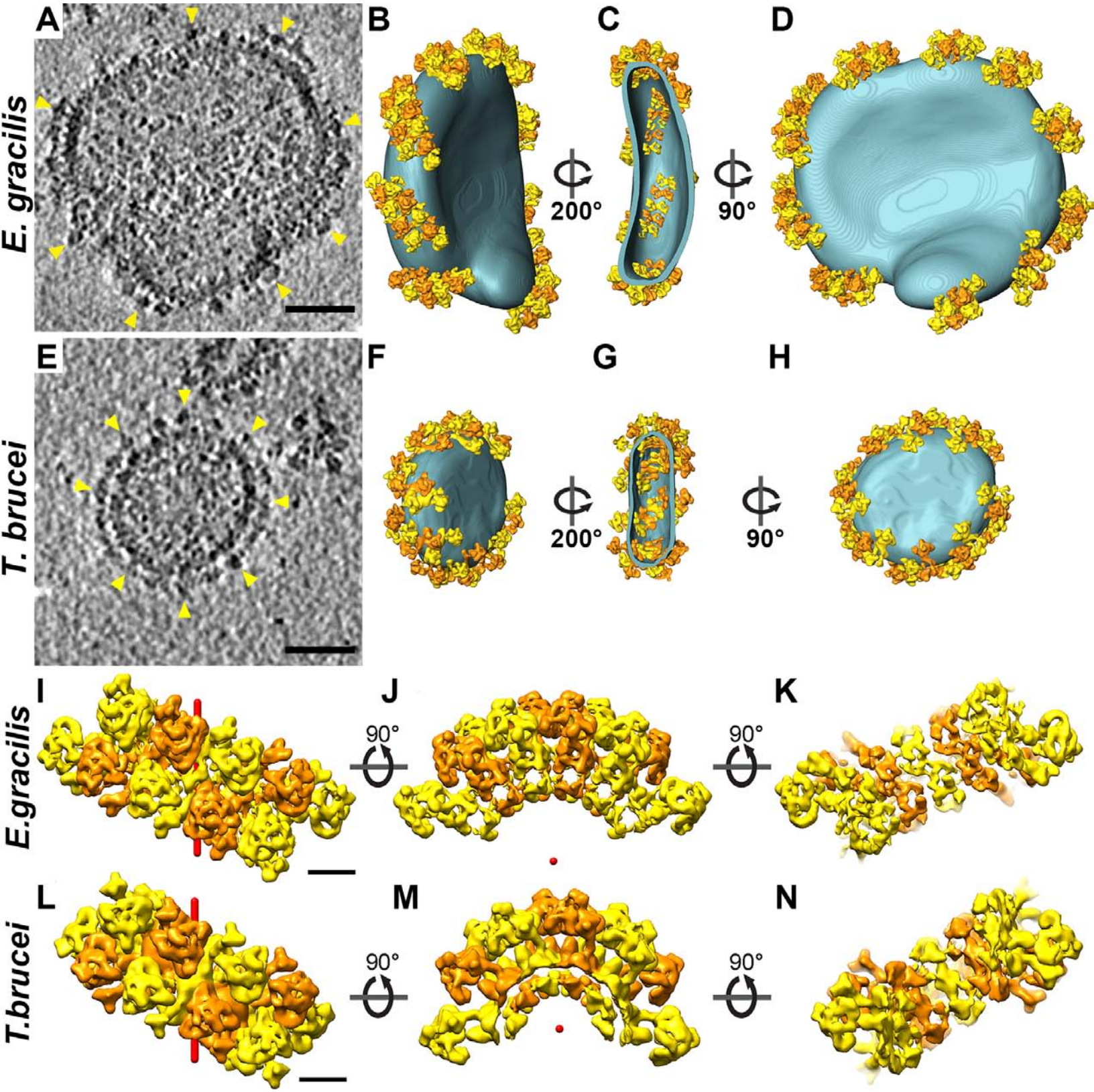
A
B
C
D
E. gracilis
200°
90°
E
F
G
H
T. brucei
200°
90°
I
J
K
E.gracilis
90°
90°
L
M
N
T.brucei
90°
90°

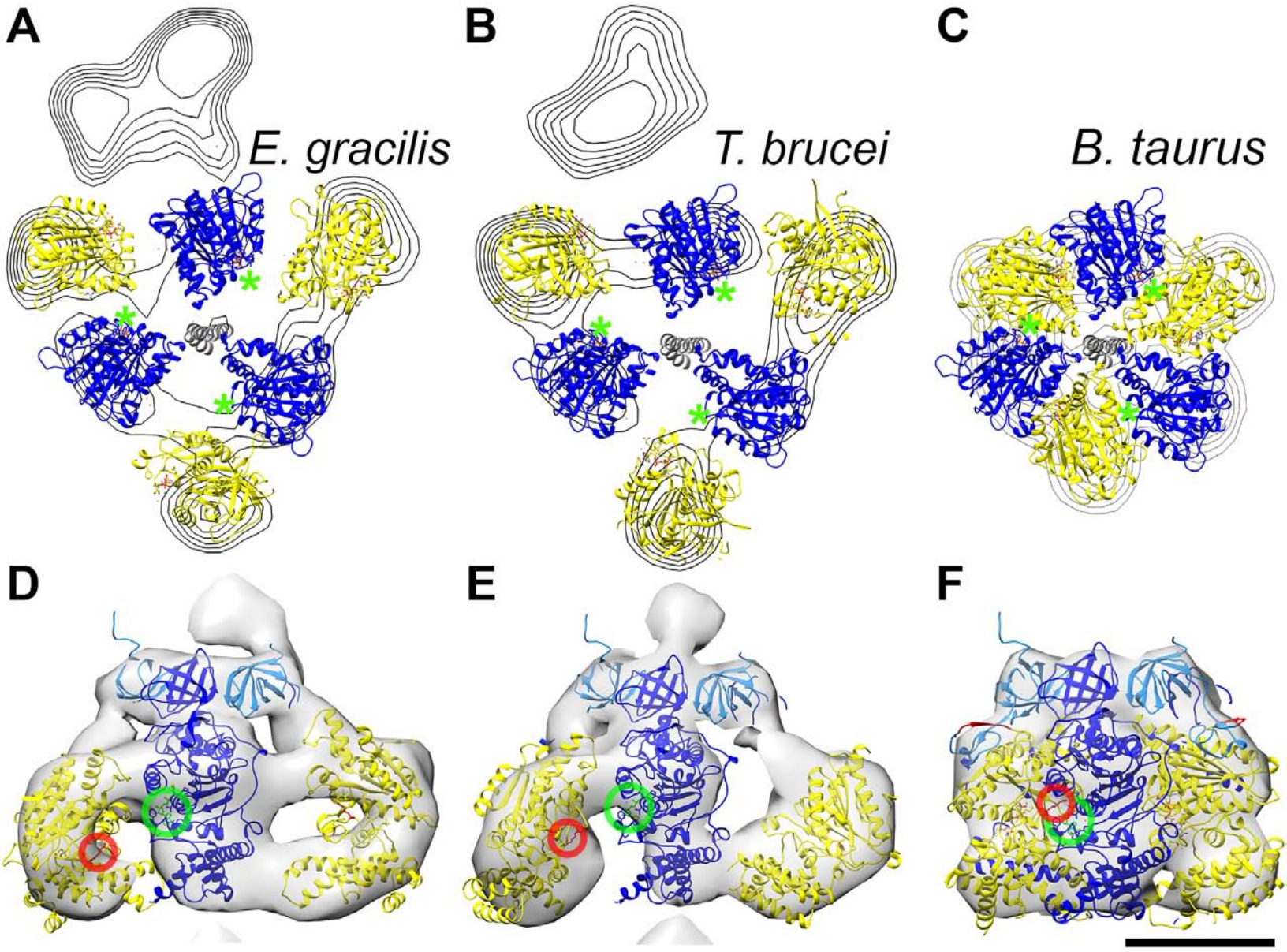
A
B
C
E. gracilis
T. brucei
B. taurus
D
E
F